MCP Papers in Press. Published on January 20, 2018 as Manuscript RA117.000370

A model of dormant-emergent metastatic breast cancer progression enabling exploration of biomarker signatures

Clark Amanda M[1], Kumar Manu P[2], Wheeler Sarah E[1], Young Carissa L[2^], Venkataramanan Raman[1,3], Stolz Donna B [1,4,6],Griffith Linda G[2], Lauffenburger Douglas A[2], Wells Alan[1,5,7*]

[*]Corresponding Author: S713 Scaife Hall
3550 Terrace St
Pittsburgh PA 15261
wellsa@upmc.edu

[1]Department of Pathology, University of Pittsburgh, Pittsburgh PA

[2]Department of Biological Engineering, Massachusetts Institute of Technology, Cambridge MA

[3]Department of Pharmaceutical Sciences, University of Pittsburgh, Pittsburgh PA

[4]Department of Cell Biology, University of Pittsburgh, Pittsburgh PA

[5]McGowan Institute for Regenerative Medicine, University of Pittsburgh, Pittsburgh PA

[6]University of Pittsburgh Cancer Center, Pittsburgh, PA

[7]Pittsburgh VA Medical Center, VA Pittsburgh Healthcare System, Pittsburgh PA

[^]Current address: [^]Applied BioMath, LLC, Lincoln MA

Running title: Biomarkers of dormant and emergent breast cancer

Abbreviations:

ALT	alanine transaminase
AST	aspartate aminotransferase
AUC	area under the curve
bFGF	basic fibroblast growth factor
BUN	blood urea nitrogen
CYP	cytochrome
EGF	epidermal growth factor
EGFR	epidermal growth factor receptor
EMT	epithelial to mesenchymal transition
G-CSF	granulocyte-colony stimulating factor
GLU	glucose
Gro	growth-regulated oncogene
HB-EGF	heparin-binding EGF-like growth factor
Hep	hepatocyte
HGF	hepatocyte growth factor
IL	interleukin
IP-10	interferon gamma-induced protein 10
IPA	Ingenuity pathway analysis
LoD	limit of detection
LPS	lipopolysaccharide
MCP	monocyte chemoattractant protein
MFI	mean fluorescent intensity
MIG	monokine induced by gamma interferon
MIP	macrophage Inflammatory Protein
MPS	microphysiological system
NPC	non-parenchymal cell

PAI-1	plasminogen activator inhibitor-1
PBS	phosphate buffered saline
PECAM-1	platelet and endothelial cell adhesion molecule 1
PLGF	placental growth factor
RANTES	regulated on activation, normal T cell expressed and secreted
RFP	red fluorescent protein
ROC	receiver operator curve
SDF	stromal cell-derived factor
sTIE-2	secreted tyrosine-protein kinase receptor
TECK	thymus-expressed chemokine
TGF	transforming growth factor
TNBC	triple-negative breast cancer
TNF	tumor necrosis factor
uPA	urokinase plasminogen activator
VEGF	vascular endothelial growth factor
WE	William's E
PAI-1	plasminogen activator inhibitor-1

SUMMARY

Breast cancer mortality predominantly results from dormant micrometastases that emerge as fatal outgrowths years after initial diagnosis. In order to gain insights concerning factors associated with emergence of liver metastases, we recreated spontaneous dormancy in an all-human *ex vivo* hepatic microphysiological system (MPS). Seeding this MPS with small numbers (<0.05% by cell count) of the aggressive MDA-MB-231 breast cancer cell line, two populations formed: actively proliferating ('growing'; EdU^+), and spontaneously quiescent ('dormant'; EdU^-). Following treatment with a clinically standard chemotherapeutic, the proliferating cells were eliminated and only quiescent cells remained; this residual dormant population could then be induced to a proliferative state ('emergent'; EdU^+) by physiologically-relevant inflammatory stimuli lipopolysaccharide (LPS) and epidermal growth factor (EGF). Multiplexed proteomic analysis of the MPS effluent enabled elucidation of key factors and processes that correlated with the various tumor cell states, and candidate biomarkers for actively proliferating (either primary or secondary emergence) versus dormant metastatic cells in liver tissue. Dormancy was found to be associated with signaling reflective of cellular quiescence even more strongly than the original tumor-free liver tissue, whereas proliferative nodules presented inflammatory signatures. Given the minimal tumor burden, these markers likely represent changes in the tumor microenvironment rather than in the tumor cells. A computational decision tree algorithm applied to these signatures indicated the potential of this MPS for clinical discernment of each metastatic stage from blood protein analysis.

INTRODUCTION

Once breast cancer advances to clinically evident metastatic disease, death invariably ensues. Upon diagnosis, the vast majority of breast cancer patients present with no evidence of disseminated disease. However, tumor cells escape into the circulation early during primary tumor development (1) and in some instances establish as small, clinically silent dormant micro-metastases in secondary ectopic sites, which emerge years later as lethal, clinically overt metastatic growths (2). As a result, following removal of the primary mass, prophylactic chemotherapy is often administered to eradicate any undetected disseminated tumor cells circulating throughout the body. While this approach has reduced recurrence and mortality by a third, there is significant morbidity and even mortality in the universal application of adjuvant chemotherapy. Furthermore, the established dormant micro-metastases are typically resistant to such treatments, which mainly act upon actively cycling cells (3, 4). Triple-negative breast cancer (TNBC) is a salient example wherein 25% of patients die from recurrence within 5-years of diagnosis despite prophylactic treatment (5). With respect to ectopic sites, evidence of breast to liver metastases is particularly foreboding with a median survival of 4 – 23 months after detection (6-8).

This treatment paradox has driven the search for defined non-invasive biomarkers or molecular signatures of secondary dissemination and outgrowth. It is imperative to discern the status of these micro-metastases – whether such cells are a beginning to emerge as lethal macro-metastases or simply remaining as dormant, clinically silent cells/nodules. This is challenging as the vanishingly small number of cells at the earliest stages are unlikely to produce sufficient signals for detection within the body. It is precisely this dilution of signals that has obstructed the development of cancer screening protocols for early detection using tumor cell-derived biomarkers. We propose that it is most fruitful to detect surrogate biomarkers that reflect the homeostasis of the tumor microenvironment being one of either suppressive dormancy or active outgrowth. As the surrounding tissue will be orders of magnitude greater than the actual tumor cell count early in emergence, the dilution of candidate biomarkers in whole body fluids should be proportionally less. To date, only a

handful of reliable biomarkers have been approved (9) and these markers are usually correlative and not mechanistically related to disease in ways that would inform therapeutic options. It is difficult to predict recurrence, yet pinpointing novel biomarkers as tools for the early detection and monitoring of metastatic recurrence would be clinically beneficial.

The surrounding tumor microenvironment, particularly the inflammatory/immune system, plays a key role in regulating metastatic resistance and recurrence (10). However, our understanding of the underlying mechanisms is limited, especially with respect to the drivers of emergence. Efforts have been hindered by the absence of pre-clinical human models that simultaneously capture the complexities of the chemoresistance exhibited by dormant metastatic cells/nodules and their subsequent emergence in a physiologically relevant ectopic niche. Such models would enable discovery of candidate biomarkers mechanistically related to disease state, and evaluation of therapeutic efficacy in real-time. The latter is of particular importance as metastatic disease is presently incurable. Further, the capability to evaluate the efficacy of new therapeutics in an all-human pre-clinical context is needed to drive more rapid progress in precision medicine.

Modeling these micro-metastases requires “mesoscale’ tissues with organ-to-tumor ratios reflective of the human situation of early and often cryptic metastases. Our 3D *ex vivo* all-human microphysiological system (MPS) is thus attractive for such investigations. Using the liver as the ectopic metastatic site, we are able to establish micro-metastases in a relatively large mass of resident hepatic cells (both parenchymal and non-parenchymal [NPC]) wherein the tumor cells initially comprise <0.05% of the tissue (11, 12). Herein, we report that not only can we recreate dormant-emergent metastatic progression of breast cancer cells, but that this MPS has the potential to identify candidate biomarkers for dormant and actively outgrowing tumor cells by detecting signals derived from the metastatic tumor as an organ, including signals from both the cancer and the host tissue.

EXPERIMENTAL PROCEDURES

Cell sources

Donor matched human hepatocytes (Heps) and NPCs (including Kupffer cells, endothelial cells, stellate cells, and tissue leukocytes) were isolated from excess pathological liver specimens. Specifically, cells were isolated from the normal margins of therapeutic partial hepatectomies for metastatic carcinomas or benign diseases. Patient donors included both males and females and no discernable differences between the genders observed (supplemental Fig. S1*A*). The cells were supplied by the National Institute of Diabetes and Digestive and Kidney Diseases (NIDDK)-funded Liver Tissue and Cell Distribution System (LTCDS), which is funded by the NIH (Contract #HHSN276201200017C). The liver specimens were processed by the LTCDS and provided to investigators as separate isolations of hepatocytes and NPCs. The NPC fraction was further purified via Percoll gradients, as previously reported (13). All cells used were approved as exempted by the University of Pittsburgh Institutional Review Board.

The TNBC breast cancer cell line, MDA-MB-231, was purchased from ATCC and transfected with red fluorescent protein (RFP) as described previously (14). The cell line was maintained in RPMI 1640 supplemented with 10% heat-inactivated fetal bovine serum and 25 IU/ml penicillin and streptomycin (Gibco, Life Technologies). MDA-MB-231 were trypsinized, centrifuged and resuspended in hepatocyte maintenance medium (detailed below). The selection antibiotic for RFP expression (puromycin) was removed at least 24 hours prior to seeding into the *ex vivo* hepatic MPS on day 3.

Ex vivo *hepatic MPS*

The *ex vivo* hepatic MPS (LiverChip) was assembled as recommended by the manufacturer (CN Bio Innovations Ltd). The high impact polystyrene scaffolds (CN Bio Innovations Ltd) were coated with 1% rat tail collagen type I (BD Biosciences) in phosphate buffered saline (PBS) for 1 hour at 37 °C and then washed with PBS before placement in the *ex vivo* hepatic MPS. The functioning and bioengineering behind the MPS have been described in detail elsewhere, and describe the fluid flows and mixing of effluents (15, 16).

The system was seeded with hepatic and cancer cells and maintained as described previously (12). Briefly, hepatocytes and NPCs were seeded into the system at a 1:1 ratio (6 x 10^5 cells/scaffold) in William's Medium E (WE; Life Technologies) supplemented with the Hepatocyte Thawing and Plating Supplement Pack (Life Technologies). Cells were cultured overnight and then the medium was changed to WE supplemented with the Hepatocyte Maintenance Supplement Pack (Life Technologies). After allowing the hepatic tissue to form, the human breast cancer cells, MDA-MB-231 cells expressing RFP (500 cells/scaffold), were introduced on day 3 (experimental overview, Fig. 1*A*). Applicable cultures were treated with 1 μM doxorubicin (APP Pharmaceuticals LLC) on day 7 to 10 (72 hours) and then stimulated on day 13 to 15 (48 hours) with a combination of 1 μg/ml LPS (Sigma-Aldrich) and 20 ng/ml mouse EGF (Corning).

Clinical chemistry assays

Clinical assays for glucose (GLU), blood urea nitrogen (BUN), aspartate transaminase (AST) and alanine aminotransferase (ALT) were performed in the CLIA-certified clinical laboratories at the University of Pittsburgh Medical Center (Pittsburgh, PA) in accordance with all governmental regulations.

Cytochrome P450 assay

The activity of four cytochrome P450 (CYP) enzymes was measured using a previously validated CYP cocktail assay (17).

Multiplex immunoassays

On day 15, effluent samples were obtained for each experimental group and the signaling profiles determined. A total of 101 cytokines, chemokines, and growth factors were assayed for using the Human Group 1 panel (27-plex), Human Chemokine Panel (40-plex), Cancer Panel1 (16-plex) and Cancer Panel 2 (18-plex). Assays were completed according to the manufacturer's instructions (BioRad Laboratories), with the exception that coupled

beads, biotinylated detection antibodies, and streptavidin-phycoerythrin fluorescent reporters were diluted 2-fold. All analytes were assessed from a total volume of 50 µL neat, undiluted culture medium per multiplex panel. To attain measurements within the working range of the assay, samples were diluted 2-, 4-, 8-, 16-, 32- and 100-fold specifically for 10 cytokines (supplemental Table S3). Standard and sample diluents consisted of WE media in the presence of 0.75% bovine serum albumin (Sigma-Aldrich).

All samples and multiplex immunoassay panels were run simultaneously to avoid confounding differences from day-to-day and operator variability. Prepared arrays were assessed by the 3D suspension array system (BioRad Laboratories) utilizing xMAP technology licensed by Luminex. Data were collected with xPONENT for FLEXMAP 3D software, version 4.2 (Luminex Corporation) and results analyzed initially in BioPlex Manager software version 6.1 (BioRad Laboratories). Absolute concentrations were calculated from median fluorescence intensity (MFI) values via calibration to 15-point standard series that implemented a 2-fold serial dilution. Assay performance metrics for each analyte are summarized in supplemental Table S3.

Cancer cell detection and quantification

Images of the scaffolds were taken using an Olympus BX51 with a 2x objective (PlanApo NA = 0.08). An Olympus CCD camera along with Magnafire image acquisition software was used to acquire digital images. The percentage of MDA-MB-231-RFP$^+$ cells on the scaffolds was determined using MetaMorph software (Molecular Devices LLC). Images of the entire scaffolds were inclusively thresholded for RFP$^+$ regions and the positive region reported as a percentage of total scaffold area.

Click-iT PLUS EdU assay

Active proliferation was assessed using the Click-iT EdU Alexa Fluor 488 Imaging Kit (Life Technologies) and performed according to the manufacturer's instructions. To each applicable well, 30 µM EdU was added on day 5 or 11 (48 hours of continuous exposure)

with the complete medium change on the specified days. Scaffolds were harvested and fixed with 2% paraformaldehyde/PBS on day 7, 13 or 15 and the presence of EdU detected thereafter. Hoechst 33342 was used for nuclear staining.

Ingenuity pathway Analysis (IPA) bioinformatics analysis

IPA (version 01-04) was utilized to identify activated pathways based upon fold changes in medians between experimental groups. Core analysis was conducted upon log2 (fold change) and performed using the Ingenuity Knowledge Base (genes and endogenous chemicals) reference set, assessing both direct and indirect relationships. Species was restricted to human, and tissue and cell lines restricted to the 'liver' and 'MDA-MB-231' cell line with relaxed and stringent filters applied, respectively. Diseases and Biological Functions were utilized to identify up- or down-regulated pathways. Pathways associated with an activation z-score greater than 1.7 or less than -1.7 were considered considerably altered.

Experimental design and statistical rationale of analyses

Design: The experimental designs are outlined in Fig. 1*A* and 2*A*. For RFP quantification, 2-3 technical and 3 biological replicates were performed. Multiplex analyses were performed on 4 biological replicates for the dormant niche, 5 for the hepatic niche and 6 for both the growing and emergent niches (each of the biological replicates had one to two technical replicates). For all experimental conditions, effluent from day 15 was analyzed and the hepatic niche served as the baseline for comparisons.

Analysis of signaling data: The concentration of each analyte was quantified using the 5-parameter logistic (5 PL) model to attain optimal curve fits for standards. The weighted sum of squared errors (wSSE) was minimized using logistic regression analyses. Typically, the weights are set equal to the inverse variance, but for immunoassays, the high-response end of a curve approaches saturation of the detector thus variance is approximated more appropriately by a power function,

$$\text{variance} = A(\text{response})^B$$

where A is a function of the magnitudes of the responses and $1.0 \leq B \leq 2.0$ for immunoassays. Curve fitting techniques were completed in BioPlex Manager software version 6.1 (BioRad Laboratories). Parameters including wSSE, residual variance, and fit probability are provided (supplemental Table S3).

Statistics: All graphs and heatmaps were generated using GraphPad Prism version 7 (GraphPad Software Inc). Wilcoxon rank sum tests were performed using MATLAB version 2016b (Mathworks Inc). Analytes identified as significantly different were those with a median fold change greater than 1.5 and a p-value < 0.05. Volcano plots were generated using the ggplot2 version 2.2.1 and ggrepel (version 0.6.5) packages in R (version 3.4.0). Receiver operator characteristics (ROC) curves for area under the curve (AUC) univariate predictions were generated using the perfcurve function in MATLAB with default parameters and decision trees were fit using the fitctree function. The standard CART algorithm was used to select the best split predictor at each node with gini's diversity index as the split criterion and a minimum parent size of 2. Candidate decision trees were generated using 4-fold cross-validation and the reported error was based on the entire data set.

RESULTS

Recapitulation of dormant-emergent breast cancer metastasis progression in a liver MPS.

Key to the use of primary cell-derived organs is the functional consistency of cells over time and between donors. The demographics and characteristics of the patient donors utilized within this study are summarized in supplemental Fig. S1*A* and supplemental Table S1. Hepatic niche function and health was unaffected by patient donor background and was maintained throughout the experiments (supplemental Fig. S1*B-J*).

Experiments using the *ex vivo* hepatic MPS were conducted as outlined in Fig. 1*A*. MDA-MB-231 (labeled with RFP) cells were seeded on day 3, treated on day 7 with proliferation-targeting chemotherapy for 72 hours, left untreated for the subsequent 72 hours, and then exposed to an inflammatory stimulus on day 13 for 48 hours. Consistent with our previous

cancer work (11, 12), on day 7, four days after colonizing the hepatic niche, MDA-MB-231 cells were predominantly actively growing (RFP^+/EdU^+) with a small population of quiescent dormant cells (RFP^+/EdU^-) (Fig. 1*B,C left* panel, supplemental Fig. S2*A*, supplemental Table S2). Treatment of the MPS with chemotherapy resulted in eradication of the vast majority of actively proliferating MDA-MB-231 cells (Fig. 1*B*, supplemental Fig. S2*B*, supplemental Table S2), leaving behind non-proliferating breast cancer cells by day 13 (Fig. 1*C*, middle panel). This indicated that within the *ex vivo* hepatic niche, there was a pre-existing dormant subpopulation of the normally highly aggressive MDA-MB-231 cells as these cells had not progressed through S phase (EdU^-) prior to chemotherapy.

Suggested location for Fig. 1

Distinct from and as an advance on our previous studies (11, 12), the main question herein was to determine if these persisting cells were indeed viable, reversibly-growth arrested cells and not merely (pre-)apoptotic or senescent cells that remained trapped within the 3D hepatic tissue. To investigate this, the persisting cells were exposed to the pathophysiologically relevant inflammatory stimulus of LPS/EGF. These cues are particularly pertinent to the liver – LPS is a common portal blood contaminant from the gastrointestinal tract that fluctuates between 0.01 to 1 ng/ml within the liver (18) that can drive the outgrowth of breast cancer cells (19, 20), and EGF is a growth factor produced immediately upon damage to the liver, and all carcinomas express the EGF receptor (EGFR) and produce cognate ligands (21). Stimulation with these extracellular signals provoked the persisting cells to emerge and outgrow (RFP^+/EdU^+) (Fig 1*B,C* right panel, supplemental Fig. S2*C*, supplemental Table S2). Additionally, the phenotypes of growing, shown on day 7. and dormant, on day 13, were maintained through day 15 (supplemental Fig. S2*D*). This result demonstrated successful *ex vivo* modeling of dormant-emergent metastatic progression as seen by a breast cancer patient at the secondary ectopic site. In summary, the three metastatic states were modeled as follows: (i) actively growing (RFP^+/EdU^+) – seeding cells

on day 3 with only media changes (Fig. 1*C*, left panel); (ii) quiescent dormancy (RFP^+/EdU^-) – treating with a standard chemotherapy (doxorubicin) (Fig. 1*C*, middle panel); and (ii) outgrowing emergent (RFP^+/EdU^+) – chemotherapeutic treatment followed by stimulation (Fig. 1*C*, right panel).

Interestingly, extension of the culture period out to 29 days and treatment of emergent cells with a second round of chemotherapy on day 21 for 72 hours (with either the same [doxorubicin] or different therapy [cisplatin]), demonstrated that secondary treatment with a different chemotherapy was more effective than the original therapy (supplemental Fig. S3), further modeling the pathophysiology observed in patients where secondary treatment is more effective when the second drug is different than the first.

Differential signaling profiles of dormant and outgrowing metastatic niches in the liver MPS

Significant progress has been made in understanding cellular activity through the molecular analysis of signaling pathways (22). Circulating effluent from the metastatic MPS essentially acts as the 'blood' of the system. Sampling and assaying this medium for secreted and soluble signaling molecules enabled us to characterize the cell-to-cell crosstalk and microenvironmental homeostasis associated with each metastatic niche. Four multiplex immunoassay panels were used to analyze circulating effluent from each scenario on day 15 (i.e. growing, dormant, and emergent metastatic niches, as well as the tumor-free hepatic niche). Accounting for signal overlap between panels and levels detectable above background, a total of 77 unique analytes out of 101 were successfully measured above the limit of detection (LoD) (Fig. 2*A*,*B* supplemental Table S3 – S8; supplemental Fig. S4 – S6). Selected analytes were those with a $p < 0.05$ and a fold change > 1.5; analytes with a $p < 0.05$ but a fold change < 1.5 are not discussed but are listed in supplemental Tables S9 – S11.

First, we assessed the change in signal abundance within each metastatic scenario relative to the hepatic niche (Fig. 2*B,C*). Interestingly, the presence of a small number of growing MDA-MB-231 cells (< 1% of total cell mass) altered the signaling profile of the

hepatic niche (Fig. 2*B*, supplemental Table S9) – 34 were increased and 33 were reduced. Although the analyte levels in the small number of specimens studied (4-6 donors) did not reach statistical significance, elevations (> 1.5-fold change) of common breast cancer-associated markers (PAI-1 and RANTES) and metastatic promoters (IP-10 and MCP-2) were observed (supplemental Table S9).

Suggested location for Fig. 2

As expected, the signaling microenvironment of the dormant metastatic scenario had low and reduced levels of most analytes (Fig. 2*B,D*, supplemental Tables S9 – S11). However, the extent to which signal abundance and crosstalk between the tumor and resident hepatic cells (hepatocytes and NPCs) remained restrained in effluent sampled 5 days after chemotherapy ceased was not anticipated, particularly in comparison to the unaffected hepatic niche. Of note, 24 out of 77 signals were significantly reduced compared to the other niches (growing/emergent/hepatic) (Fig. 2*D*, supplemental Table S11). These signals encompassed breast cancer-associated markers (PAI-1, uPA, PLGF, sCD40L, MCP-1), contributors of metastasis/tumorigenesis (Gro-α/-β, HB-EGF, MIP-1α/-1β, IL-1Ra/-18/17A, TGF-α, G-CSF, HGF, IL-6) and angiogenic factors (sTIE-2, VEGF-C, endoglin, angiopoietin-2, follistatin, HB-EGF, bFGF). Although no signals were significantly elevated, a higher abundance of 3-5 analytes (> 1.5-fold change) was observed above the other niches (growing/emergent/hepatic) (supplemental Tables S9 – S11). Interestingly, PECAM-1 was elevated to a similar degree compared to all scenarios, but its importance remains unclear (Fig. 2*C*).

For a more clinically relevant assessment to detect tumors that would warrant intervention, we queried analyte abundance in the actively outgrowing tumor cells (growing and emergent metastatic niches) to that of non-proliferating (dormant and tumor-free hepatic niches) (Fig. 2*E*, supplemental Table S11). In validation of the metastatic MPS model, the majority of the significantly abundant analytes were either breast cancer-associated markers

(uPA, PAI-1, RANTES, MCP-1) or those with a strong association with breast cancer progression (IL-6, Gro-α/-β, MIP-1α, IL-1RA, SDF-1α/β, TECK, MIG).

The growing and emergent metastatic niches largely exhibited similar signaling profiles, particularly compared to the dormant metastatic niche (Fig. 2*B*, supplemental Table S10); this was expected as both situations have proliferating tumor cell nodules. For the emergent metastatic niche, stimulation returned 34 out of 41 signals that were reduced in the dormant metastatic niche following chemotherapeutic treatment (supplemental Table S9). Indeed, the emergent metastatic niche was associated with a striking abundance of analytes (Fig. 2*B,E,F*, supplemental Tables S9 – S11), suggesting that over the limited timescale herein, the stimuli that caused emergence were strong effectors. A further 15 signals were present in significantly increased quantities compared to growing untreated tumor cells (RANTES, MIP-1α/-1δ, IL-1β/-2/-5/-8/-10/-16, TGF-α, eotaxin-2/-3, MCP-3/-4, TNF-α) (Fig. 2*G*, supplemental Table S10). These signals are derived mainly from activated immune and stromal cells (23-34) collectively suggesting LPS/EGF mainly act to stimulate the resident NPCs of the liver (e.g. Kupffer, stellate and endothelial cells) which in turn cause cancer cell outgrowth, rather than acting directly on the tumor cells. Interestingly, 3 signals reported to play significant roles in angiogenesis remained significantly decreased following treatment with doxorubicin (i.e. in dormant and emergent) (HGF, sTIE-2, PLGF) (Fig. 2*F*, supplemental Table S10).

Distinct functional pathways are activated within each metastatic niche in the liver MPS

IPA was employed to investigate the systemic impact of the different signaling microenvironments within metastatic niches captured in Fig. 2. IPA predictions revealed alterations in several biological mechanisms and functions amongst the experimental metastatic stages based upon fold variations in analyte levels (Fig. 3). In validation of the metastatic MPS, analysis of the growing MDA-MB-231 cells revealed activation of cancer pathways, specifically metastasis of cells, and lipid metabolism pathways, specifically triacylglycerol concentrations (Fig. 3*A*). The applicability of metastatic cancer pathways is

evident. The latter is linked to enhanced/reactivation of lipid biosynthesis as part of cancer-associated metabolic reprogramming to glycolysis (35), which is a frequent response of metastasizing tumor cells colonizing and surviving in the liver due the low oxygen and glucose levels (36).

Suggested location for Fig. 3

Consistent with previous data, IPA indicated numerous biological pathways were downregulated in the dormant metastatic niche (Fig. 3*B,C*, supplemental Fig. S7*A*). Dramatically reduce were those associated with cell movement, migration and proliferation of cancer cells as well as the activity of resident liver cells, both parenchymal and NPCs. One pathway relating to carbohydrate synthesis was markedly unregulated (Fig. 3*B*, supplemental Fig. S7*A*). Given the negligible fraction (<0.03%) of tumor cells present in the dormant metastatic niche (Fig. 1*B*), synthesis of carbohydrates is likely a response of the resident liver cells as the liver plays an important role in regulating carbohydrate homeostasis (37). The accumulation of glycogen in hepatocytes is another mark of a 'quiet' liver.

Substantiating findings in Fig. 2*F,G*, actively outgrowing tumor cells (growing and emergent metastatic niches) were linked to breast cancer cell line migration and movement as well as mitosis (Fig. 3*B,C*, supplemental Fig. S7*C*); behaviors that mark the mesenchymal transition in tumor cells, and which is consistent with the secondary epithelial-to-mesenchymal-transition (EMT) that correlates with emergence (38). Further, stimulation of the immune system was predicted to be the key pathway associated with the emergent MDA-MB-231 cells, specifically the recruitment, migration, activation and quantity of cells from the myeloid lineage (Fig. 3*C,D,* supplemental Fig. S7*B*). Pathways associated with liver damage were activated in emergent metastatic niche, likely a direct result of the stimulation applied and unlikely to reflect the microenvironmental contribution to emergence.

Univariate analysis distinguished candidate biomarkers/signatures of dormant and outgrowing metastatic stages

For diagnostic purposes, we postulated that molecular signatures reflective of cellular dormancy or activated outgrowth should be based upon the homeostasis of the tumor microenvironment, rather than the tumor cells. The percentage of tumor cells during the initial stages of metastasis and their notorious genetic heterogeneity make identifying markers derived from tumor cells exceeding difficult. To evaluate the power of each analyte to act as a candidate biomarker indicative of metastatic niches containing outgrowing and dormant tumor cells, we calculated the AUC under the ROC curve using each analyte present in the circulating effluent as a univariate predictor. Lists of selected and ranked molecules capable of discriminating between these outcomes are presented in Fig. 4.

Suggested location for Fig. 4

Analysis identified 21 candidate biomarkers of an outgrowing metastatic niche, all with high AUC values (> 0.75, $p < 0.05$) (Fig. 4*A*). Consistent with previous results for the outgrowing metastatic niche, many analytes that exhibited high predictive ability are established breast cancer-associated biomarkers, notably uPA (0.96; 95% CI, 0.65 – 0.93)**,** Gro-α (0.88; 95% CI, 0.57 – 0.94), MIG (0.83; 95% CI, 0.63 – 0.92), PAI-1 (0.80; 95% CI, 0.44 – 0.90) and RANTES (0.79; 95% CI, 0.50 – 0.91). Meanwhile, 9 analytes demonstrated high sensitivity for the restrained microenvironment of a dormant metastatic niche with an inverse AUC > 0.90 (Fig. 4*B*). Fifteen of the candidate biomarkers for the outgrowing metastatic niche were also inversely diagnostic for dormant metastatic niches (Fig. 4*A,B* - bold).

Potential of diagnostic decision tree models of signaling proteins to accurately stage the metastatic niche of the liver MPS

To further explore the clinical utility of the metastatic MPS, possible decisions trees for diagnosis were constructed to identify the crucial mediators and cut-offs of metastatic stages based upon the levels of soluble and secreted molecules in Fig. 2. The utility of decision trees is to identify prediction rules from data and then illustrate them as a binary tree where each terminal node (leaf) corresponds to a class or other nodes which represent measured variables. Three decision trees diagnosed each metastatic niche created with the immortalized MDA-MB-231 cells line from the tumor-free hepatic niche with a predictive accuracy of 100%, 95.2%, and 85.7%, respectively (Fig. 4*C,D,E*). The molecular classifiers for the emergent metastatic niche were associated with high discriminatory power (TGF-α [1.0; 95% CI 0.66 – 1.00], MIP-1α [0.92; 95% CI 0.50 – 1.00], and G-CSF [0.93; 95% CI 0.36 – 0.96]) as were the dormant molecular classifiers (bFGF [0.10; 95% CI 0.06 – 0.35]), while the growing molecular classifiers were associated with moderate discriminatory power (uPA [0.78; 95% CI 0.41 – 0.94], MIG [0.77; 95% CI 0.54 – 0.86]) (supplemental Table S12).

Overall, these data demonstrated that profiling the circulating effluent from the metastatic MPS can discriminate between livers that contain dormant or outgrowing (either primary or secondary emergence) breast cancer cells. While the accuracy of the decisions trees generated are very high, this is not unexpected given the limited numbers of samples and consistency of experimentation, given that the MPS system is robust and relevant to cancer progression. Thus, these serve as examples that require refinement with a diversity of primary cancer cells and subsequent validation in human specimens.

DISCUSSION

Metastatic breast cancer remains a largely incurable and fatal disease. The danger stems from tumor cells that disseminate early and lay as clinically silent, dormant cells/nodules, which may awaken to outgrow after a long and variable period of latency. These metastatic relapses occur in only one-third or fewer women who received a seemingly curative removal of the primary tumor. In the absence of our ability to detect these disseminations early, adjuvant systemic treatments are provided blindly, with significant

iatrogenic morbidity and even mortality. Further, the disseminated cells, either nodules or small micro-metastatic outgrowths, are generally resistant to therapies compounding this clinical challenge (3, 4). This underscores the need to determine whether micro-metastases are present, and if the nodules are in a dormant, chemoresistant state or early outgrowth which could portend a window of therapeutic efficacy.

Herein, we presented an all-human 3D *ex vivo* hepatic MPS to model dormant-emergent metastasis in a critical organ involved in lethal metastases (for a wide range of cancers). This is proposed to overcome the lack of pre-clinical models that reliably recreate dormancy, particularly without genetic or pharmacologic interventions. The metastatic MPS presented contains a complete complement of liver cells, including those of the immune/inflammatory system (Kupffer cells, stellate cells, liver sinusoidal endothelial cells and tissue leukocytes), which can be colonized by a limiting number of breast cancer cells (<0.05%). The value of the system is shown by the spontaneous attainment of dormancy, with a fraction undergoing a transition to an epithelial quiescence, tunable upon altering the physical properties of the MPS (11). The metastatic MPS was stable for over a month and modeled the dormant-emergent metastatic progression observed in breast cancer patients: (i) breast cancer cells spontaneously enter quiescent dormancy, (ii) proliferating cells were eliminated by standard chemotherapies, while quiescent dormant cells remained, and (iii) surviving cells were reversibly-quiescent as they could emerge and outgrow following a physiologically-relevant inflammatory stimulus. This system captured the essential properties that define cellular dormancy – survival in foreign microenvironments, reversible growth arrest and resistance to cytotoxic agents (2-4). Those of emergence were also attained in that the dormant cells could be simulated to re-enter the cell cycle. Moreover, this demonstrated that dormant cells were not senescent or pre-apoptotic but viable, quiescent cells. To our knowledge, this was the first time that dormant-emergent progression, representing recurrence, has been demonstrated *ex vivo* in an organ-on-a-chip system – previous studies, including our own, have all focused on the earlier events of the metastatic cascade (*e.g.* invasion, angiogenesis, intravasation, extravasation, and colonization) (39).

This defined system, with cancer micro-metastases of predictable phenotypes (growing, dormant or emergent), allowed us to seek biomarkers that can be obtained in a minimally invasive manner. Through multiplexed profiling of the circulating effluent (system blood mimetic) we could discriminate between livers that contained dormant or outgrowing (either primary or secondary emergence) breast cancer cells. Livers housing dormant cells presented a signaling fingerprint reflective of non-inflammatory quiescence with almost the complete set of signaling molecules lower than in the uninvolved liver tissue. Meanwhile, livers housing the growing and emergent nodules moved in lockstep with inflammatory signatures. Overall, the signals were associated with pathways consistent with either suppression or activation of a mitogenic and motogenic tumor cell phenotype, and inflamed and reparative local environment in the case of emergent tumor cells.

Emergence from dormancy is the most clinically relevant phase. Changes in the microenvironment that disrupt the stable dormant state are likely responsible. Recent studies identified stromal cells, particularly endothelial cells and macrophages, as playing a role in controlling dormancy and emergence in the liver, bone, lung and brain (40-43), In accordance with these studies, our data suggests that the signals driving emergence likely derive from the resident liver NPCs (e.g. Kupffer, stellate and liver sinusoidal endothelial cells) (23-32, 34). This is not surprising given that both pathophysiological stressors, LPS and EGF, are potent stimulators of these resident liver cell populations (31, 44-47). We posit that the stimuli that lead to emergence necessitate a process wherein inflammatory stimuli directly stimulate the stromal cells within the metastatic niche, which produce the signals responsible for awakening reversibly quiescent, dormant breast cancer cells. Further, it was anticipated that the signaling microenvironments of emergent and growing metastatic stages would be different, but also exhibit similarity as they are both actively growing. The emergent metastatic stage diverged with respect to signal abundance and the aforementioned additional presence of signals typically produced by immune cells. These key differences stemmed from the underlying biology and microenvironments wherein a stimulus was required for emergent outgrowth. This aligns with our premise that it is advantageous to

base molecular biomarkers for detection and characterization of micro-metastases upon the homeostasis of the tumor microenvironment as the markers likely derive from the tissue resident cells rather than tumor intrinsic signals. This is surmised not only because of the minimal comparative mass of the macro-metastases but the markedly reduced signaling profile associated with livers housing dormant nodules below that of tissue alone. Further, that many markers are reduced under selected conditions (such as dormancy) necessitates that these derive from the liver mass as the limiting dilution of tumor cells do not offset the number of hepatic cells. The contributions of the tumor cells to upregulated signals would be, if anything, less than noted in humans as the systemic dilution of signals within the MPS is likely greater than that observed in human (human body the cell-to-blood ratios is ~ $5x10^9$:1 (48), while in the LiverChip it is $7.5x10^5$:1). However, one needs to be cognizant that signals in the MPS effluent are not taken up, or scavenged by other organs or cells in circulation. Thus, the exact levels in comparison to human specimens await clinical correlation studies. The definitive elucidation of signal origins and specific instigators of emergence remain for future investigations.

There is promise that this can be applied clinically as we could define biomarkers with high AUC values, and generate diagnostic decision tree models discerning each metastatic stage. Most all of the molecules identified have been associated with metastases (being detected at the later, less treatable stage of macro-metastases) and reduced overall survival. However, it is premature to discuss specific biomarkers at present as the AUC values and decision trees currently serve as proofs of principle. This is for a number of reasons. First, herein we used a singular cancer cell line, of a specific subtype (the highly recurrent triple negative phenotype). Second, the dilutional and isolated organ issues addressed above will impact the translation to the clinical situation. However, that highly predictive decision trees can be readily obtained argues for moving forward with further biomarker studies. Importantly, we emphasize this is a validation of 'fit for purpose' and are not stating the molecules listed within are new candidates to be considered for clinical use. Moreover, we acknowledge our model unlikely to translate in all aspects because of the low

predictive power caused by the small donor number. Validation in animals is not readily attainable due to the lack of reliable and tunable spontaneous dormancy models, the stochastic nature of true metastases from primary tumor growths, and the inability to control emergence. Translation to persons will be hampered by the long latency between primary tumors and metastatic recurrence. Still, the predictability of the MPS suggests that a future clinical utility involves the incorporation and investigation of patient-derived cells post-hoc. Lastly, it must be noted that many of the identified factors may be causative for emergence and not merely indicative, which could provide for interventions to prevent outgrowth.

This MPS approximates the earliest, and clinically silent stages of metastatic seeding, dormancy, outgrowth and emergence in an all human context and thus captures this situation uniquely from animal models and human specimens, but it is still not without significant limitations. The cellular complement is complex and but not fully complete lacking some of the hematopoietic immune cells that would populate such an invaded liver, and the connections to other organs that would modify any tissue responses. Further, the time-scale of days to weeks rather than months to years would also impact extrapolation to the patient situation. Thus, any signatures or potentially causal linkages would need to be validated in human specimens; the decision tree analyses presented herein only serve to demonstrate that unique signatures may be possible. Given the daunting challenges of validation in that the specimens would need to be assessed in the absence of knowledge about whether any given patient even harbored micrometastases, such prior work in a tractable system such as this one, is requisite to focus the translational study. Further, we feel that this system can also be used as a first step in therapeutic interventions to determine whether potential causal signals are valid targets for further study.

The future utility of this metastatic MPS is innumerable. It is easily adaptable to other cancer types, such as metastatic prostate (49) or metastatic colorectal cancer, which has an abysmal 5-year survival of only 10% (50). This model is also poised to capture many of the relevant features of inflammation-mediated tumor outgrowth. New iterations extend to a multi-organ MPS (51), which connects the metastatic hepatic niche to relevant inflammatory

organs, to further pursue drivers of emergence, such as the gut (52) or adipose fat (53) as well as to a primary tumor to model the entire metastatic cascade from the initial escape through to immediate outgrowth or delayed emergence at the secondary ectopic site. Moreover, MPSs are making large strides in bridging the gap between bench level pre-clinical experiments and clinical trials in humans (15, 54-57). As the liver is the principle site of drug metabolism, the MPS may also serve as an all-human model to replace mice in the pre-clinical evaluation of therapies against recurrence that eradicate or maintain a dormant state turning metastasis into chronic, manageable disease.

Acknowledgements

The work described within is funded by grants from the NIH (5UH3TR000496-05), a VA Merit Award, and DARPA (BAA-11-73 Microphysiological Systems: W911NF-12-2-0039).

REFERENCES

1. Husemann, Y., Geigl, J. B., Schubert, F., Musiani, P., Meyer, M., Burghart, E., Forni, G., Eils, R., Fehm, T., Riethmuller, G., and Klein, C. A. (2008) Systemic spread is an early step in breast cancer. *Cancer. Cell.* 13, 58-68
2. Weinberg, R. A. (2008) The many faces of tumor dormancy. *APMIS.* 116, 548-551
3. Gonzalez-Angulo, A. M., Morales-Vasquez, F., and Hortobagyi, G. N. (2007) Overview of resistance to systemic therapy in patients with breast cancer. *Adv. Exp. Med. Biol.* 608, 1-22
4. Ma, B., Wheeler, S. E., Clark, A. M., Whaley, D. L., Yang, M., and Wells, A. (2016) Liver protects metastatic prostate cancer from induced death by activating E-cadherin signaling. *Hepatology* 64, 1725-1742
5. Kalimutho, M., Parsons, K., Mittal, D., Lopez, J. A., Srihari, S., and Khanna, K. K. (2015) Targeted Therapies for Triple-Negative Breast Cancer: Combating a Stubborn Disease. *Trends. Pharmacol. Sci.* 36, 822-846

6. Ge, Q. D., Lv, N., Kong, Y. N., Xie, X. H., He, N., Xie, X. M., and Wei, W. D. (2012) Clinical characteristics and survival analysis of breast cancer molecular subtypes with hepatic metastases. *Asian. Pac. J. Cancer. Prev.* 13, 5081-5086
7. Lobbezoo, D. J., van Kampen, R. J., Voogd, A. C., Dercksen, M. W., van den Berkmortel, F., Smilde, T. J., van de Wouw, A. J., Peters, F. P., van Riel, J. M., Peters, N. A., de Boer, M., Borm, G. F., and Tjan-Heijnen, V. C. (2013) Prognosis of metastatic breast cancer subtypes: the hormone receptor/HER2-positive subtype is associated with the most favorable outcome. *Breast. Cancer. Res. Treat.* 141, 507-514
8. O'Reilly, S. M., Richards, M. A., and Rubens, R. D. (1990) Liver metastases from breast cancer: the relationship between clinical, biochemical and pathological features and survival. *Eur. J. Cancer.* 26, 574-577
9. Harris, L. N., Ismaila, N., McShane, L. M., Andre, F., Collyar, D. E., Gonzalez-Angulo, A. M., Hammond, E. H., Kuderer, N. M., Liu, M. C., Mennel, R. G., Van Poznak, C., Bast, R. C., Hayes, D. F., and American Society of Clinical, O. (2016) Use of Biomarkers to Guide Decisions on Adjuvant Systemic Therapy for Women With Early-Stage Invasive Breast Cancer: American Society of Clinical Oncology Clinical Practice Guideline. *J. Clin. Oncol.* 34, 1134-1150
10. Linde, N., Fluegen, G., and Aguirre-Ghiso, J. A. (2016) The Relationship Between Dormant Cancer Cells and Their Microenvironment. *Adv. Cancer. Res.* 132, 45-71
11. Clark, A. M., Wheeler, S. E., Young, C. L., Stockdale, L., Shepard Neiman, J., Zhao, W., Stolz, D. B., Venkataramanan, R., Lauffenburger, D., Griffith, L., and Wells, A. (2016) A liver microphysiological system of tumor cell dormancy and inflammatory responsiveness is affected by scaffold properties. *Lab. Chip.* 17, 156-168
12. Wheeler, S. E., Clark, A. M., Taylor, D. P., Young, C. L., Pillai, V. C., Stolz, D. B., Venkataramanan, R., Lauffenburger, D., Griffith, L., and Wells, A. (2014) Spontaneous dormancy of metastatic breast cancer cells in an all human liver microphysiologic system. *Br. J. Cancer.* 111, 2342-2350

13. Hwa, A. J., Fry, R. C., Sivaraman, A., So, P. T., Samson, L. D., Stolz, D. B., and Griffith, L. G. (2007) Rat liver sinusoidal endothelial cells survive without exogenous VEGF in 3D perfused co-cultures with hepatocytes. *FASEB. J.* 21, 2564-2579
14. Chao, Y. L., Shepard, C. R., and Wells, A. (2010) Breast carcinoma cells re-express E-cadherin during mesenchymal to epithelial reverting transition. *Mol. Cancer.* 9, 179
15. Clark, A. M., Ma, B., Taylor, D. L., Griffith, L., and Wells, A. (2016) Liver metastases: Microenvironments and ex-vivo models. *Exp. Biol. Med. (Maywood)* 241, 1639-1652
16. Clark, A. M., Wheeler, S. E., Taylor, D. P., Pillai, V. C., Young, C. L., Prantil-Baun, R., Nguyen, T., Stolz, D. B., Borenstein, J. T., Lauffenburger, D. A., Venkataramanan, R., Griffith, L. G., and Wells, A. (2014) A microphysiological system model of therapy for liver micrometastases. *Experimental biology and medicine* 239, 1170-1179
17. Pillai, V. C., Strom, S. C., Caritis, S. N., and Venkataramanan, R. (2013) A sensitive and specific CYP cocktail assay for the simultaneous assessment of human cytochrome P450 activities in primary cultures of human hepatocytes using LC-MS/MS. *J. Pharm. Biomed. Anal.* 74, 126-132
18. Lumsden, A. B., Henderson, J. M., and Kutner, M. H. (1988) Endotoxin levels measured by a chromogenic assay in portal, hepatic and peripheral venous blood in patients with cirrhosis. *Hepatology* 8, 232-236
19. De Cock, J. M., Shibue, T., Dongre, A., Keckesova, Z., Reinhardt, F., and Weinberg, R. A. (2016) Inflammation Triggers Zeb1-Dependent Escape from Tumor Latency. *Cancer. Res.* 76, 6778-6784
20. Yang, H., Wang, B., Wang, T., Xu, L., He, C., Wen, H., Yan, J., Su, H., and Zhu, X. (2014) Toll-like receptor 4 prompts human breast cancer cells invasiveness via lipopolysaccharide stimulation and is overexpressed in patients with lymph node metastasis. *PLoS One.* 9, e109980
21. Wells, A. (1999) EGF receptor. *Int. J. Biochem. Cell. Biol.* 31, 637-643
22. Scott, J. D., and Pawson, T. (2009) Cell signaling in space and time: where proteins come together and when they're apart. *Science* 326, 1220-1224

23. Adams, D. H., Hubscher, S., Fear, J., Johnston, J., Shaw, S., and Afford, S. (1996) Hepatic expression of macrophage inflammatory protein-1 alpha and macrophage inflammatory protein-1 beta after liver transplantation. *Transplantation* 61, 817-825
24. Connolly, M. K., Bedrosian, A. S., Malhotra, A., Henning, J. R., Ibrahim, J., Vera, V., Cieza-Rubio, N. E., Hassan, B. U., Pachter, H. L., Cohen, S., Frey, A. B., and Miller, G. (2010) In hepatic fibrosis, liver sinusoidal endothelial cells acquire enhanced immunogenicity. *J. Immunol.* 185, 2200-2208
25. Gregory, S. H., and Wing, E. J. (2002) Neutrophil-Kupffer cell interaction: a critical component of host defenses to systemic bacterial infections. *J. Leukoc. Biol.* 72, 239-248
26. Gressner, A. M., and Chunfang, G. (1995) A cascade-mechanism of fat storing cell activation forms the basis of the fibrogenic reaction of the liver. *Verh. Dtsch. Ges. Pathol.* 79, 1-14
27. Heydtmann, M., Hardie, D., Shields, P. L., Faint, J., Buckley, C. D., Campbell, J. J., Salmon, M., and Adams, D. H. (2006) Detailed analysis of intrahepatic CD8 T cells in the normal and hepatitis C-infected liver reveals differences in specific populations of memory cells with distinct homing phenotypes. *J. Immunol.* 177, 729-738
28. Inra, C. N., Zhou, B. O., Acar, M., Murphy, M. M., Richardson, J., Zhao, Z., and Morrison, S. J. (2015) A perisinusoidal niche for extramedullary haematopoiesis in the spleen. *Nature* 527, 466-471
29. Lewindon, P. J., Pereira, T. N., Hoskins, A. C., Bridle, K. R., Williamson, R. M., Shepherd, R. W., and Ramm, G. A. (2002) The role of hepatic stellate cells and transforming growth factor-beta(1) in cystic fibrosis liver disease. *Am. J. Pathol.* 160, 1705-1715
30. Leyland, H., Gentry, J., Arthur, M. J., and Benyon, R. C. (1996) The plasminogen-activating system in hepatic stellate cells. *Hepatology* 24, 1172-1178
31. Liebe, R., Breitkopf-Heinlein, K., Waldow, K., Braun, S., Thomas, M., Schildberg, F., Knolle, P., Zanger, U., Klingmüller, U., and Ebert, M. (2015) Mouse hepatic stellate cells

are responsive to LPS and contribute to the acute phase response of hepatocytes. *Z. Gastroenterol.* 53, A1_37

32. Liu, C., Huang, X., Werner, M., Broering, R., Ge, J., Li, Y., Liao, B., Sun, J., Peng, J., Lu, M., Hou, J., and Zhang, X. (2017) Elevated Expression of Chemokine CXCL13 in Chronic Hepatitis B Patients Links to Immune Control during Antiviral Therapy. *Front. Immunol.* 8
33. Mosher, B., Dean, R., Harkema, J., Remick, D., Palma, J., and Crockett, E. (2001) Inhibition of Kupffer cells reduced CXC chemokine production and liver injury. *J. Surg. Res.* 99, 201-210
34. Stefanovic, L., Brenner, D. A., and Stefanovic, B. (2005) Direct hepatotoxic effect of KC chemokine in the liver without infiltration of neutrophils. *Exp. Biol. Med. (Maywood)* 230, 573-586
35. Baenke, F., Peck, B., Miess, H., and Schulze, A. (2013) Hooked on fat: the role of lipid synthesis in cancer metabolism and tumour development. *Dis. Model. Mech.* 6, 1353-1363
36. Dupuy, F., Tabaries, S., Andrzejewski, S., Dong, Z., Blagih, J., Annis, M. G., Omeroglu, A., Gao, D., Leung, S., Amir, E., Clemons, M., Aguilar-Mahecha, A., Basik, M., Vincent, E. E., St-Pierre, J., Jones, R. G., and Siegel, P. M. (2015) PDK1-Dependent Metabolic Reprogramming Dictates Metastatic Potential in Breast Cancer. *Cell. Metab.* 22, 577-589
37. Postic, C., Dentin, R., and Girard, J. (2004) Role of the liver in the control of carbohydrate and lipid homeostasis. *Diabetes. Metab.* 30, 398-408
38. Wells, A., Yates, C., and Shepard, C. R. (2008) E-cadherin as an indicator of mesenchymal to epithelial reverting transitions during the metastatic seeding of disseminated carcinomas. *Clin. Exp. Metastasis.* 25, 621-628
39. Caballero, D., Kaushik, S., Correlo, V. M., Oliveira, J. M., Reis, R. L., and Kundu, S. C. (2017) Organ-on-chip models of cancer metastasis for future personalized medicine: From chip to the patient. *Biomaterials* 149, 98-115

40. Ghajar, C. M., Peinado, H., Mori, H., Matei, I. R., Evason, K. J., Brazier, H., Almeida, D., Koller, A., Hajjar, K. A., Stainier, D. Y., Chen, E. I., Lyden, D., and Bissell, M. J. (2013) The perivascular niche regulates breast tumour dormancy. *Nat. Cell. Biol.* 15, 807-817
41. Lu, X., and Kang, Y. (2007) Organotropism of breast cancer metastasis. *Journal of mammary gland biology and neoplasia* 12, 153-162
42. Taylor, D. P., Clark, A., Wheeler, S., and Wells, A. (2014) Hepatic nonparenchymal cells drive metastatic breast cancer outgrowth and partial epithelial to mesenchymal transition. *Breast. Cancer. Res. Treat.* 144, 551-560
43. Yang, M., Ma, B., Shao, H., Clark, A. M., and Wells, A. (2016) Macrophage phenotypic subtypes diametrically regulate epithelial-mesenchymal plasticity in breast cancer cells. *BMC Cancer.* 16, 419
44. Knolle, P. A., Loser, E., Protzer, U., Duchmann, R., Schmitt, E., zum Buschenfelde, K. H., Rose-John, S., and Gerken, G. (1997) Regulation of endotoxin-induced IL-6 production in liver sinusoidal endothelial cells and Kupffer cells by IL-10. *Clin. Exp. Immunol.* 107, 555-561
45. Komposch, K., and Sibilia, M. (2015) EGFR Signaling in Liver Diseases. *Int. J. Mol. Sci.* 17
46. Su, G. L. (2002) Lipopolysaccharides in liver injury: molecular mechanisms of Kupffer cell activation. *Am. J. Physiol. Gastrointest. Liver. Physiol.* 283, G256-265
47. Lanaya, H., Natarajan, A., Komposch, K., Li, L., Amberg, N., Chen, L., Wculek, S. K., Hammer, M., Zenz, R., Peck-Radosavljevic, M., Sieghart, W., Trauner, M., Wang, H., and Sibilia, M. (2014) EGFR has a tumour-promoting role in liver macrophages during hepatocellular carcinoma formation. *Nat. Cell. Biol.* 16, 972-981, 971-977
48. Sender, R., Fuchs, S., and Milo, R. (2016) Revised Estimates for the Number of Human and Bacteria Cells in the Body. *PLoS biology* 14, e1002533
49. Yates, C., Shepard, C. R., Papworth, G., Dash, A., Beer Stolz, D., Tannenbaum, S., Griffith, L., and Wells, A. (2007) Novel three-dimensional organotypic liver bioreactor to directly visualize early events in metastatic progression. *Adv. Cancer. Res.* 97, 225-246

50. Goldberg, R. M., Rothenberg, M. L., Van Cutsem, E., Benson, A. B., 3rd, Blanke, C. D., Diasio, R. B., Grothey, A., Lenz, H. J., Meropol, N. J., Ramanathan, R. K., Becerra, C. H., Wickham, R., Armstrong, D., and Viele, C. (2007) The continuum of care: a paradigm for the management of metastatic colorectal cancer. *The oncologist* 12, 38-50
51. Chen, W. L. K., Edington, C., Suter, E., Yu, J., Velazquez, J. J., Velazquez, J. G., Shockley, M., Large, E. M., Venkataramanan, R., Hughes, D. J., Stokes, C. L., Trumper, D. L., Carrier, R. L., Cirit, M., Griffith, L. G., and Lauffenburger, D. A. (2017) Integrated Gut/Liver Microphysiological Systems Elucidates Inflammatory Inter-Tissue Crosstalk. *Biotechnol. Bioeng.*
52. Round, J. L., and Mazmanian, S. K. (2009) The gut microbiota shapes intestinal immune responses during health and disease. *Nat. Rev. Immunol.* 9, 313-323
53. Nieman, K. M., Romero, I. L., Van Houten, B., and Lengyel, E. (2013) Adipose tissue and adipocytes support tumorigenesis and metastasis. *BBA* 1831, 1533-1541
54. Caplin, J. D., Granados, N. G., James, M. R., Montazami, R., and Hashemi, N. (2015) Microfluidic Organ-on-a-Chip Technology for Advancement of Drug Development and Toxicology. *Adv. Healthc. Mater.* 4, 1426-1450
55. Low, L. A., and Tagle, D. A. (2017) Organs-on-chips: Progress, challenges, and future directions. *Exp. Biol. Med. (Maywood)*, 1535370217700523
56. Wikswo, J. P. (2014) The relevance and potential roles of microphysiological systems in biology and medicine. *Exp. Biol. Med. (Maywood)* 239, 1061-1072
57. Yu, J., Cilfone, N. A., Large, E. M., Sarkar, U., Wishnok, J. S., Tannenbaum, S. R., Hughes, D. J., Lauffenburger, D. A., Griffith, L. G., Stokes, C. L., and Cirit, M. (2015) Quantitative Systems Pharmacology Approaches Applied to Microphysiological Systems (MPS): Data Interpretation and Multi-MPS Integration. *CPT. Pharmacometrics. Syst. Pharmacol.* 4, 585-594

FIGURE LEGENDS

Fig. 1: Modeling dormant-emergent metastatic breast cancer in the hepatic niche. (A) Schematic depicting the experimental outline. (B) The percent presence of MDA-MB-231 cells (RFP^+) per scaffold on day 7, on day 13 after treatment with 1 μM doxorubicin (72 hours), and on day 15 following stimulation with 1 μg/mL lipopolysaccharide (LPS) + 20 ng/mL epidermal growth factor (EGF) (n = 3 donors, 2-3 replicates per donor, mean ± SEM). (C) Representative images of growing (Hep/NPC + MDA-MB-231), dormant (Hep/NPC + MDA-MB-231 + doxorubicin) and emergent (Hep/NPC + MDA-MB-231 + doxorubicin + LPS/EGF) MDA-MB-231 cells in the hepatic niche on day 7, 13 and 15, respectively. Red – MDA-MB-231 cells; green – EdU; blue – Hoechst. Scale bar – top panel 200 μm, bottom panel 50 μm. Significant differences were determined via non-parametric Wilcoxon rank sum tests (***$p < 0.001$).

Fig. 2: Signaling profiles from growing, dormant and emergent metastatic breast cancer cells in the hepatic niche. Levels of 77 unique analytes cytokines, chemokines and cancer-related signaling factors in day 15 effluent from MPS cultures of the hepatic niche and three metastatic experimental MDA-MB-231 stages [hepatic niche (n = 5 donors, 1-2 replicates per donor), growing (n = 6 donors, 1-2 replicates per donor), dormant (n = 4 donors, 1-2 replicates per donor) and emergent metastatic niches (n = 6 donors, 1-2 replicates per donor)] were determined. (A) Schematic depicting the experimental outline. (B) Heatmap depicting individual signal abundance in the metastatic experimental MDA-MB-231 niches relative to the hepatic niche for each donor (fold change in absolute concentrations (pg/ml), log2 transformation). Red – growing metastatic niche; green – dormant metastatic niche; blue – emergent metastatic niche. (C) Venn diagram presenting all signals produced in a higher abundance relative to the hepatic niche. (D-G) Volcano plots summarize significantly altered analytes (red) determined as those exhibiting fold changes > 1.5 and $p < 0.05$. (D) Dormant metastatic niche compared to growing/emergent/hepatic niches. (E) Emergent metastatic niche compared to growing/dormant/hepatic niches. (F)

Emergent metastatic niche compared to the growing metastatic niche. (G) Outgrowing MDA-MB-231 cells (emergent/growing metastatic niche) compared to non-proliferating (dormant/hepatic niche).

Fig. 3: Activated biological pathways in the dormant-emergent metastatic MPS identified by IPA. Tables detailing activated pathways identified via IPA for designated metastatic experimental niche comparisons. (A) Growing metastatic niche compared to the hepatic niche. (B) Dormant metastatic niche compared to the growing metastatic niche. Emergent metastatic niche compared to (C) dormant and (D) growing metastatic niches.

Fig. 4: Candidate biomarkers and decision trees discerning metastatic breast cancer niches in the hepatic MPS. Diagnostic accuracy of signals for (A) actively proliferating experimental metastatic breast cancer (growing and emergent) and non-proliferating scenarios (dormant and hepatic niche) and (B) dormant metastatic breast cancer based AUC analyses. (C-E) Three decision tree models generated discerned the different emergent, growing and dormant experimental metastatic breast cancer stages using signal concentrations from system blood mimetic (i.e. effluent). Number cut-offs are based upon pg/mL levels. (C) TNF-α > uPA > bFGF (21/21 correct, 100% accuracy). (D) MIP-1α > uPA > bFGF (20/21 correct, 95.2% accuracy). (E) G-CSF > MIG > bFGF (18/21 correct, 85.7% accuracy). Significant differences were determined via non-parametric Wilcoxon rank sum tests (*$p < 0.05$, **$p < 0.01$, ***$p < 0.001$).

Figure 1.

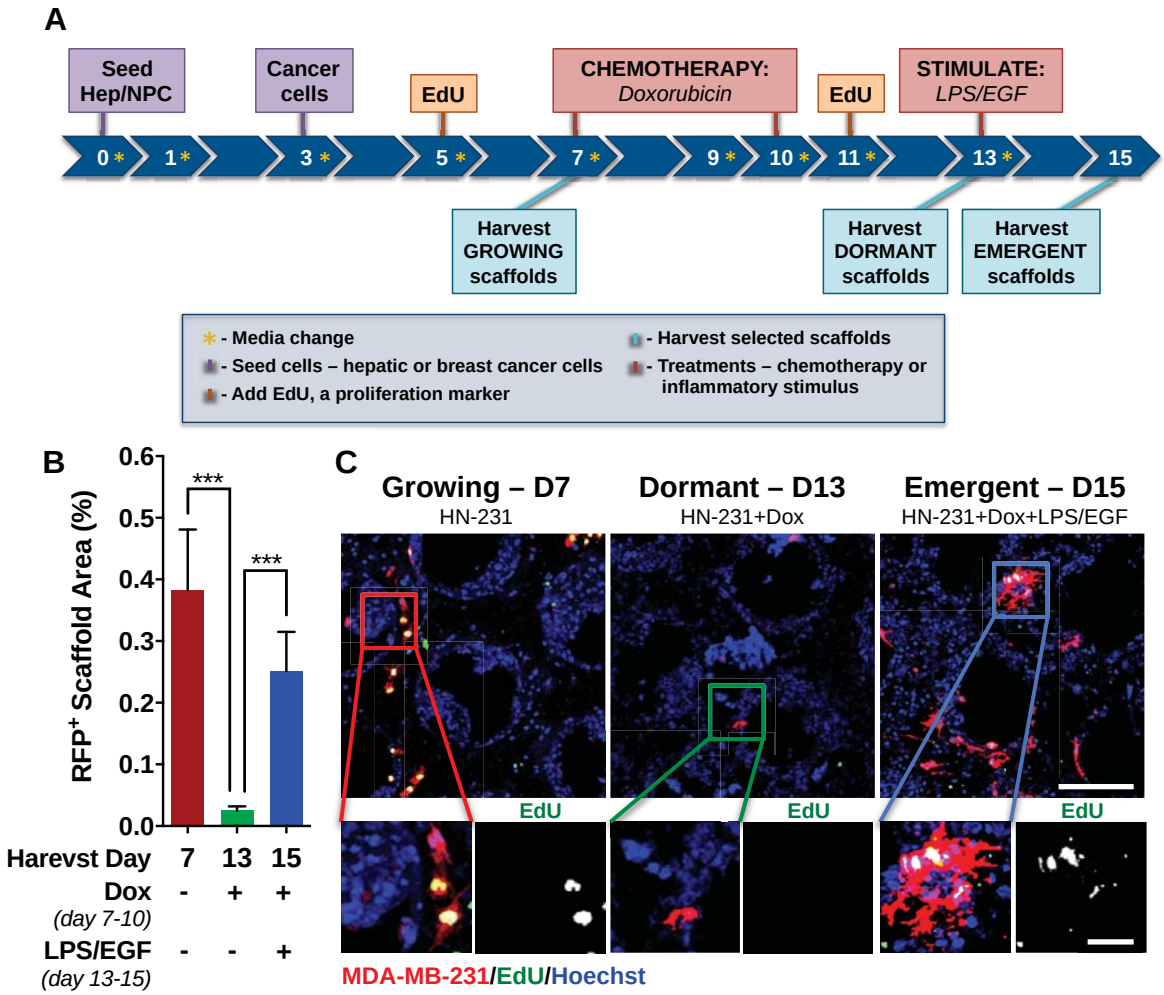

Figure 2.

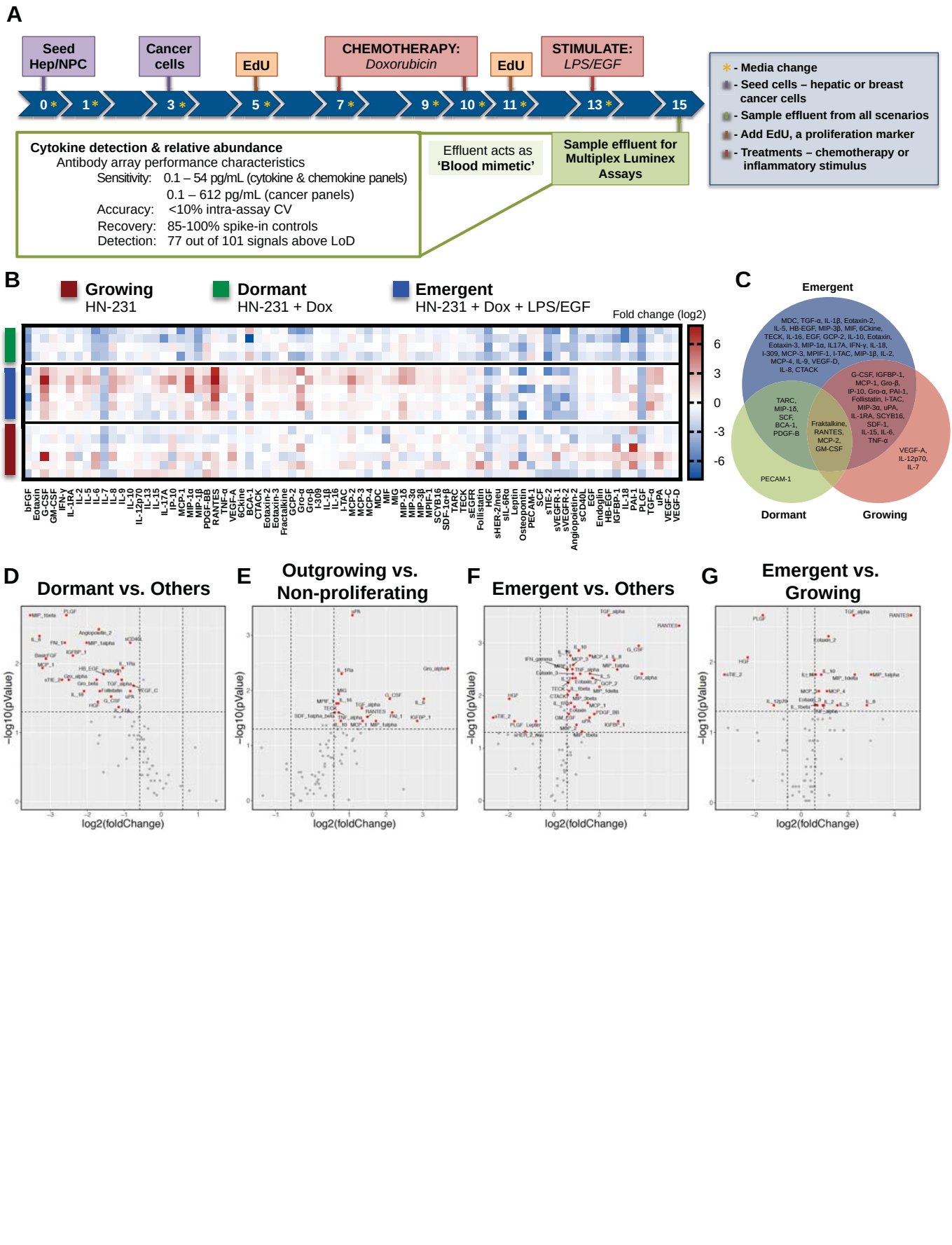

Figure 3.

A

Growing vs. HN		
Function Annotation	**z-score**	**No.**
Cancer		
metastasis of cells	1.98	4
Lipid Metabolism		
concentration of triacylglycerol	1.71	6

B

Dormant vs. Growing		
Function Annotation	**z-score**	**No.**
Carbohydrate Metabolism		
synthesis of carbohydrate	1.96	4
Cellular Movement		
migration of cells	-3.96	22
cell movement	-3.89	23
migration of breast cancer cell lines	-3.12	15
cell movement of liver cells	-2.96	9
cell movement of breast cancer cell lines	-2.93	17
cell movement of hepatic stellate cells	-2.60	7
chemotaxis	-2.19	5
leukocyte migration	-2.18	8
Hepatic System Development and Function		
regeneration of liver	-2.77	12
stimulation of liver cells	-2.75	8
migration of liver cells	-2.61	7
stimulation of hepatocytes	-2.58	7
migration of hepatic stellate cells	-2.20	5
proliferation of liver cells	-2.15	20
proliferation of hepatocytes	-2.09	15
activation of liver cells	-1.98	15
Cellular Growth and Proliferation		
cell proliferation of breast cancer cell lines	-2.75	11
proliferation of blood cells	-2.21	5
Cell Death and Survival		
cell viability	-2.59	7
cell viability of liver cells	-1.95	4
Cell Cycle		
mitosis	-2.41	6
mitogenesis of liver cells	-2.21	5
mitosis of hepatocytes	-2.00	4
Hematological System Development and Function		
quantity of leukocytes	-2.39	6
quantity of lymphocytes	-1.94	4
Cell-To-Cell Signaling and Interaction		
recruitment of phagocytes	-2.24	5
recruitment of myeloid cells	-2.24	5
binding of breast cancer cell lines	-2.18	5
activation of blood cells	-1.98	5
activation of leukocytes	-1.98	4
activation of cells	-1.91	18
activation of myeloid cells	-1.72	4
DNA Replication, Recombination, and Repair		
synthesis of DNA	-1.89	10

C

Emergent vs. Dormant		
Function Annotation	**z-score**	**No.**
Cellular Movement		
migration of cells	2.59	22
cell movement	2.49	23
migration of breast cancer cell lines	2.46	15
recruitment of phagocytes	2.24	5
recruitment of myeloid cells	2.24	5
chemotaxis	2.19	5
cell movement of breast cancer cell lines	1.71	17
Hematological System Development and Function		
quantity of leukocytes	2.39	6
quantity of lymphocytes	1.94	4
Cellular Development		
differentiation of cells	2.20	5
Hepatic System Development and Function		
damage of liver	2.00	18
Cell-To-Cell Signaling and Interaction		
activation of blood cells	1.98	5
activation of leukocytes	1.98	4
activation of myeloid cells	1.72	4
Cell Cycle		
mitosis	1.84	6

D

Emergent vs. Growing		
Function Annotation	**z-score**	**No.**
Cellular Movement		
recruitment of phagocytes	2.24	5
recruitment of myeloid cells	2.24	5
leukocyte migration	1.99	8
Hepatic System Development and Function		
damage of liver	2.18	18
Cell-To-Cell Signaling and Interaction		
activation of blood cells	1.98	5
activation of leukocytes	1.98	4
activation of myeloid cells	1.72	4
Hematological System Development and Function		
quantity of leukocytes	1.76	4

Figure 4.

A

Outgrowing Analyte	AUC	95% CI	*p*-value	
uPA	**0.96**	**(0.65 - 0.93)**	**0.0004**	***
Gro-α	**0.88**	**(0.57 - 0.94)**	**0.004**	**
IL-1RA	**0.87**	**(0.57 - 0.92)**	**0.005**	**
MIG	0.83	(0.63 - 0.92)	0.012	*
G-CSF	0.82	(0.47 - 0.85)	0.014	*
IL-6	**0.82**	**(0.57 - 0.94)**	**0.014**	*
IL-16	**0.81**	**(0.59 - 0.95)**	**0.017**	*
MPIF-1	**0.81**	**(0.64 - 0.95)**	**0.017**	*
TGF-α	**0.81**	**(0.53 - 0.92)**	**0.021**	*
TNF-α	**0.80**	**(0.53 - 0.92)**	**0.025**	*
SDF-1α/β	**0.80**	**(0.53 - 0.91)**	**0.025**	*
TECK	**0.80**	**(0.60 - 0.94)**	**0.025**	*
PAI-1	**0.80**	**(0.44 - 0.90)**	**0.025**	*
RANTES	0.79	(0.50 - 0.91)	0.030	*
IL-10	0.78	(0.61 - 0.93)	0.036	*
MCP-1	**0.78**	**(0.59 - 0.93)**	**0.036**	*
MIP-1α	**0.78**	**(0.50 - 0.92)**	**0.036**	*
IGFBP-1	**0.78**	**(0.63 - 0.99)**	**0.036**	*
GM-CSF	0.77	(0.59 - 0.91)	0.043	*
6Ckine	0.77	(0.57 - 0.93)	0.043	*
Eotaxin-3	0.77	(0.65 - 0.94)	0.043	*

B

Dormant Analyte	AUC	95% CI	*p*-value	
MIP-1β	0.00	(0.00 - 0.18)	0.0027	**
PLGF	0.00	(0.05 - 0.32)	0.0027	**
sCD40L	0.01	(0.00 - 0.15)	0.0036	**
MIP-1α	**0.03**	**(0.06 - 0.33)**	**0.0048**	**
Angiopoietin-2	0.03	(0.00 - 0.24)	0.0048	**
PAI-1	**0.03**	**(0.06 - 0.40)**	**0.0048**	**
uPA	**0.04**	**(0.04 - 0.37)**	**0.0063**	**
IL-6	**0.04**	**(0.04 - 0.30)**	**0.0063**	**
MCP-1	**0.04**	**(0.00 - 0.17)**	**0.0063**	**
Endoglin	0.06	(0.00 - 0.21)	0.0082	**
HB-EGF	0.06	(0.00 - 0.19)	0.0082	**
VEGF-D	0.06	(0.00 - 0.22)	0.0082	**
IL-1RA	**0.07**	**(0.06 - 0.35)**	**0.011**	*
Gro-α	**0.07**	**(0.08 - 0.34)**	**0.011**	*
TGF-α	**0.07**	**(0.01 - 0.29)**	**0.011**	*
VEGF-C	0.07	(0.00 - 0.24)	0.011	*
IGFBP-1	**0.09**	**(0.00 - 0.27)**	**0.014**	*
IL-16	**0.09**	**(0.01 - 0.31)**	**0.014**	*
bFGF	0.10	(0.06 - 0.35)	0.016	*
IL-18	0.10	(0.00 - 0.28)	0.018	*
G-CSF	0.12	(0.12 - 0.44)	0.022	*
Gro-β	0.13	(0.02 - 0.35)	0.028	*
SDF-1α/β	**0.13**	**(0.06 - 0.33)**	**0.028**	*
Follistatin	0.13	(0.11 - 0.40)	0.028	*
VEGF-A	0.15	(0.04 - 0.37)	0.035	*
MPIF-1	**0.15**	**(0.04 - 0.35)**	**0.035**	*
TECK	**0.15**	**(0.05 - 0.40)**	**0.035**	*
sTIE-2	0.15	(0.05 - 0.35)	0.035	*
IL-5	0.16	(0.04 - 0.46)	0.044	*
IL-17A	0.16	(0.05 - 0.43)	0.044	*
TNF-α	**0.16**	**(0.07 - 0.35)**	**0.044**	*
CTACK	0.16	(0.06 - 0.34)	0.044	*
MCP-4	0.16	(0.04 - 0.32)	0.044	*
EGF	0.17	(0.00 - 0.32)	0.049	*

C

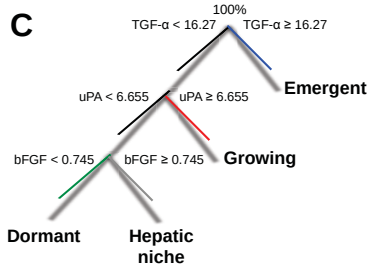

D

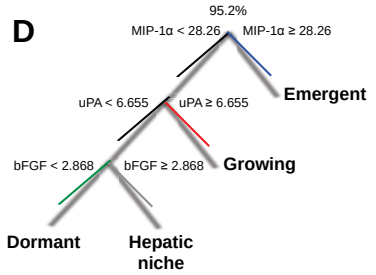

E